C. R. Palevol 16 (2017) 585–599

Contents lists available at ScienceDirect

Comptes Rendus Palevol

www.sciencedirect.com

Human Palaeontology and Prehistory

Adaptation to bipedal gait and fifth metatarsal structural properties in *Australopithecus*, *Paranthropus*, and *Homo*

Adaptation à la marche bipède et propriétés structurales du cinquième métatarse chez Australopithecus, Paranthropus *et* Homo

Mark R. Dowdeswell [a], Tea Jashashvili [b,c,d,*], Biren A. Patel [e,f,d], Renaud Lebrun [g], Randall L. Susman [h], David Lordkipanidze [c], Kristian J. Carlson [e,d,i,j]

[a] *School of Statistics and Actuarial Science, University of the Witwatersrand, Johannesburg, South Africa*
[b] *Molecular Imaging Center, Department of Radiology, USC Keck School of Medicine, University of Southern California, Los Angeles, USA*
[c] *Department of Geology and Palaeontology, Georgian National Museum, Tbilisi, Georgia*
[d] *Evolutionary Studies Institute, University of the Witwatersrand, Johannesburg, South Africa*
[e] *Department of Cell and Neurobiology, Keck School of Medicine, University of Southern California, Los Angeles, USA*
[f] *Human and Evolutionary Biology Section, Department of Biological Sciences, University of Southern California, Los Angeles, USA*
[g] *Institut des Sciences de l'Evolution de Montpellier – UMR 5554, Montpellier, France*
[h] *Department of Anatomical Sciences, Stony Brook University, Stony Brook, USA*
[i] *School of Geosciences, University of the Witwatersrand, Johannesburg, South Africa*
[j] *Department of Anthropology, Indiana University, Bloomington, USA*

ARTICLE INFO

Article history:
Received 11 August 2016
Accepted after revision 24 October 2016
Available online 2 December 2016
Handled by Roberto Macchiarelli and Clément Zanolli

Keywords:
Bone functional adaptation
Foot loading
Lateral column
Hominoids
Visualization

ABSTRACT

Humans, unlike African apes, have relatively robust fifth metatarsals (Mt5) presumably reflecting substantial weight-bearing and stability function in the lateral column of the former. When this morphological difference emerged during hominin evolution is debated. Here we investigate internal diaphyseal structure of Mt5s attributed to *Australopithecus* (from Sterkfontein), *Paranthropus* (from Swartkrans), and *Homo* (from Olduvai, Dmanisi, and Dinaledi) placed in the context of human and African ape Mt5 internal diaphyseal structure. 'Whole-shaft' properties were evaluated from 17 cross sections sampling 25% to 75% diaphyseal length using computed tomography. To assess structural patterns, scaled cortical bone thicknesses (sCBT) and scaled second moments of area (sSMA) were visualized and evaluated through penalized discriminant analyses. While the majority of fossil hominin Mt5s exhibited ape-like sCBT, their sSMA were comparatively more human-like. Human-like functional loading of the lateral column existed in at least some fossil hominins, although perhaps surprisingly not in hominins from Dmanisi or Dinaledi.

Mots clés :
Adaptation fonctionnelle de l'os
Répartition du poids sur le pied
Partie latérale du pied
Hominoïdes
Visualisation

RÉSUMÉ

Contrairement aux grands singes, les humains ont un cinquième métatarse (Mt5) robuste. Cette morphologie particulière est liée au fait qu'une plus grande partie du poids du corps repose sur la partie latérale du pied. La date de l'émergence de ce caractère au cours de l'évolution humaine est toujours sujette à débats. Nous étudions ici la structure interne de la diaphyse du Mt5 chez les genres *Australopithecus* (de Sterkfontein), *Paranthropus*

* Corresponding author at: Molecular Imaging Center, Department of Radiology, USC Keck School of Medicine, University of Southern California, Los Angeles, USA.
E-mail address: tjashashvili@yahoo.fr (T. Jashashvili).

http://dx.doi.org/10.1016/j.crpv.2016.10.003
1631-0683/

(de Swartkrans) et *Homo* (d'Olduvai, de Dinaledi et de Dmanisi), que nous comparons à l'homme moderne ainsi qu'aux grands singes africains. Nous avons utilisé la tomographie afin d'évaluer les propriétés des diaphyses dans leur ensemble à partir de 17 sections transversales de celles-ci, effectuées entre 25 % et 75 % de la longueur totale de l'os. Afin d'évaluer les patrons structurels de ce métatarse, l'épaisseur calibrée de l'os (sCBT) ainsi que l'épaisseur calibrée des moments quadratiques (sSMA) ont été mesurées, puis comparées au sein de l'échantillon par analyse discriminante pondérée. Alors que la majorité des fossiles d'hominidés ont des valeurs de sCBT pour Mt5 similaires à celles observées pour les grands singes actuels, les valeurs de sSMA sont proches de celles de l'homme actuel. Chez certains hominidés fossiles au moins, à l'instar de l'homme moderne, la partie latérale du pied supportait une fraction importante du poids du corps, bien que, de manière peut-être surprenante, ce ne soit pas le cas pour les homininés de Dmanisi et de Dinaledi.

1. Introduction

The foot is functionally comprised of medial and lateral columns (Morton, 1935), the latter of which includes the fourth and fifth rays (e.g., metatarsals along with their associated phalanges). Proximally, fourth and fifth metatarsals (Mt4 and Mt5, respectively) articulate with the cuboid, which in turn articulates with the calcaneus. Greater rigidity in the lateral column, including within metatarsophalangeal, tarsometatarsal, and calcaneocuboid joints, is a functionally distinguishing characteristic of the modern human foot that is correlated with the presence of longitudinal and transverse arches, all of which enable the human foot to serve more effectively and efficiently as a stiff lever during the last half of stance phase in terrestrial gaits (DeSilva, 2010; Elftman and Manter, 1935a,b; Hicks, 1954; Jones, 1941; Ker et al., 1987; Lewis, 1980b; Morton, 1922, 1924; Susman, 1983). Apes, on the other hand, exhibit less arching and tend to exhibit greater sagittal plane movement in mid-foot joints during the last half of stance phase in terrestrial gaits (Elftman and Manter, 1935a; Gebo, 1992; Nowak et al., 2010; Susman, 1983; Vereecke et al., 2003). This joint movement has been referred to as a "mid-tarsal break" (Bojsen-Møller, 1979; Nowak et al., 2010) or "mid-foot break" (DeSilva, 2010). Greater mid-foot joint mobility in apes presumably reflects selection for greater conformity of the foot to substrates, particularly arboreal ones (Gebo, 1992).

The modern human foot experiences the highest loads during stance phase in its medial column (e.g., first metatarsal, Mt1), while loads lessen progressively in increasingly more lateral metatarsals (Stokes et al., 1979; Wearing et al., 2001). Within-individual load variability applied to lateral metatarsals also has been shown to be less than that applied to medial metatarsals in humans (Wearing et al., 2001). Using a theoretical approach, Preuschoft (1969) reasoned that dorsoplantar and mediolateral oriented bending moments differentiated Mt1 and Mt5 loading, respectively. In comparisons of plantar pressure associated with terrestrial quadrupedal and bipedal gaits, and specifically the path of the centre of pressure over the course of stance phase, some of these findings have been corroborated by different pressure distributions and patterns beneath the foot of humans and apes (D'Août et al., 2004; Vereecke et al., 2003). Bonobos exhibit a centre of pressure that remains more laterally-positioned over a longer period of stance phase during terrestrial quadrupedal and bipedal gaits compared to that of bipedal humans, and also a centre of pressure that fluctuates more in the mediolateral direction than typically observed in humans (De Cock et al., 2008; Hayafune et al., 1999; Nagel et al., 2008; Vereecke et al., 2003). Chimpanzees exhibit a relatively more laterally-positioned centre of pressure than humans during late stance phase and push-off (Elftman and Manter, 1935b). And gorillas, while less well-studied than other African apes, appear to exhibit relatively more laterally-positioned high plantar pressure than humans during stance phase (Crompton et al., 2012). Collectively, these studies of terrestrial gaits provide strong evidence of loading differences between the medial and lateral columns of modern humans versus those of apes.

Several external features of non-hallucal metatarsals highlight important functional differences between the lateral column of modern human and ape feet. For example, African apes show more internal torsion (inversion) of Mt3, Mt4, and Mt5 heads, while humans show more external torsion (eversion) of Mt3, Mt4, and Mt5 heads (Drapeau and Harmon, 2013). African apes exhibit plantar angulation of metatarsal diaphyses relative to the base in the lateral column whereas humans exhibit a dorsal angulation (Lewis, 1980a). Humans emphasize dorsal doming of metatarsal heads coupled with transverse guttering separating the subchondral surface of the head from the diaphysis, whereas apes exhibit a flatter dorsal surface without transverse guttering (Fernández et al., 2015, 2016; Latimer and Lovejoy, 1990; Susman, 1983). Finally, humans tend to exhibit an Mt5 that is second in robustness to Mt1, whereas apes tend to exhibit Mt5s with the lowest diaphyseal robusticity within the metatarsus (Archibald et al., 1972; Day and Napier, 1964; Marchi, 2010; Pontzer et al., 2010; Susman, 1988). All of these features combine to demonstrate selective pressures on modern human foot adaptations favouring obligate terrestrial bipedalism.

In contrast to comparisons of external morphology, internal structural comparisons between modern human and ape metatarsal diaphyses are comparatively less well-documented. This is despite internal properties, such as cortical bone thickness and second moments of area, that exhibit good correspondence with comparative foot biomechanics in humans and apes (Jashashvili et al., 2015; Marchi, 2005, 2010). When these internal evaluations have been made, typically they have been theoretical

(Preuschoft, 1969), restricted to single diaphyseal locations such as midshaft (Griffin and Richmond, 2005; Griffin et al., 2008; Marchi, 2005), or estimated using a robusticity index that relies on external dimensions (Day and Napier, 1964; Harcourt-Smith et al., 2015; Pontzer et al., 2010; Zipfel et al., 2009). Other approaches for quantifying and comparing internal structure, such as evaluating continuous diaphyseal (i.e. 'whole-shaft') cross-sectional properties, ultimately may be equally or even more informative for identifying bone functional adaptations that signal mechanical loading differences (Carlson and Marchi, 2014a; Ruff et al., 2006). For example, Jashashvili and colleagues (2015) investigated whether human versus ape plantar pressure pattern differences, and presumed loading scenarios, are manifested in continuous internal diaphyseal structure in the Mt1, and indeed significant differences were observed in the form of a greater emphasis on resisting dorsoplantarly-oriented bending loads in humans compared to African apes. Whether similar structural details are evident in metatarsal diaphyses of the lateral column (e.g., Mt5) is uncertain. The first goal of the present study is to investigate continuous diaphyseal internal structure of modern human and African ape metatarsals in the lateral column of the foot (i.e. Mt5s) in order to visualize and quantify the extent of their similarities and differences, as recently performed for the medial column (i.e. Mt1s) (Jashashvili et al., 2015).

While unique features of the human foot, presumably reflecting its unique loading patterns during bipedalism, were thought to have evolved fairly early during hominin evolution because of their mechanically selective benefits to bipedalism (Harcourt-Smith et al., 2015; Ward et al., 2011), it is worth re-evaluating this proposition given recent studies documenting kinematic variability in the human foot, including the presence of a well-defined mid-tarsal break in some individuals (Bates et al., 2013; Crompton et al., 2012; DeSilva and Gill, 2013; DeSilva et al., 2015; Greiner and Ball, 2014). These observations have important evolutionary implications since they suggest that the configuration of the human foot may not be as constrained to be universally rigid during bipedal gaits as commonly assumed. Moreover, it is noteworthy that during stance phase of bipedal gaits the feet of habitually unshod humans exhibit greater conformity with the substrate (as suggested by greater uniformity in peak pressures of the foot) compared to the feet of habitually shod individuals (D'Août et al., 2009). However, despite a burgeoning recognition of kinematic variability exhibited by modern human feet, there remain clear functional differences when comparing medial or lateral columns of human versus ape feet.

On several grounds, it has been proposed that human-like function in the lateral column of the hominin foot preceded the appearance of human-like function in its medial column (Kidd, 1998, 1999; Morton, 1935; Proctor, 2013). An early appearance in the hominin fossil record of metatarsal features that have been associated with modern human-like lateral column stability, such as evidence of arching in the foot of *Australopithecus afarensis* and *A. africanus*, supports its selective importance to a biped (Ward et al., 2011; Zipfel et al., 2009). The selective importance of these external morphological configurations also is supported by their persistence over the course of early hominin evolution, as indicated by a number of outwardly similar fossil hominin Mt5s (e.g., AL 333-13, AL 333-78, SKX 33380, StW114/115, OH 8, and KNM-ER 803f; Day and Napier, 1964; Susman, 1988; Zipfel et al., 2009). In support of this, Proctor (2013) also argued for functional conservatism within the lateral column by demonstrating through a 3D geometric morphometric analysis of the Mt5 proximal articular surface that the form of humans, apes, and fossil hominins could not be readily distinguished. While these lines of evidence may collectively suggest relative stasis in functional morphology of hominin Mt5s, such a view would seem to be at odds with the growing trend towards emphasizing bipedal kinematic mosaicism in early hominins (DeSilva et al., 2013; Haile-Selassie et al., 2012; Hatala et al., 2016; Lovejoy et al., 2009; Zipfel et al., 2011). In support of this trend, recent studies of internal structure in the hominin tibiotalar joint (Su and Carlson, 2015; Su et al., 2013) suggest that *Paranthropus* may have exhibited a more modern human-like medial weight shift during the last half of stance phase, while other hominins such as *A. africanus*, like apes, appear to have retained a relatively more lateral centre of pressure during the last half of stance phase. In light of the accumulating evidence supporting this trend, as well as the possibility that using single midshaft comparisons of Mt5s may be too coarse a means of conducting a comparative approach (e.g., Marchi, 2005), we predict that structural differences in hominin metatarsal internal structure may exist, including within the Mt5, and that it would be useful to contextualize them within structural differences exhibited by modern humans and apes (e.g., Jashashvili et al., 2015). Thus, the second goal of the present study is to investigate continuous diaphyseal internal structure of several hominin Mt5s in order to visualize and quantify the extent of their uniformity, as well as their similarities to and differences from human and ape Mt5s.

In this study, we investigate internal diaphyseal structure of the Mt5 in order to shed new light on the extent to which modern humans and African apes differ. We visualize and quantify differences in two structural parameters – cortical bone thickness and second moments of area – that have previously been shown to differentiate continuous diaphyseal structure of human, chimpanzee, and gorilla Mt1s (Jashashvili et al., 2015). We predict that human Mt5s differ from those of chimpanzees and gorillas, with the former emphasizing dorsoplantarly-oriented loading. We also visualize and quantify the same structural parameters in several Mt5s attributed to *Australopithecus*, *Paranthropus*, and *Homo*, and apply the comparative framework in order to assess the extent of hominin variability in Mt5 diaphyseal structure. In doing this, we test the hypothesis of functional conservatism in the lateral column of the hominin foot. If differences between hominin Mt5s are observed, we predict that *Australopithecus* Mt5s should be more African ape-like in diaphyseal structure compared to fossil *Homo* Mt5s because of the apparent absence of a medial weight shift in the last half of stance in the former. We predict that *Paranthropus* Mt5s should be more modern human-like because of the apparent presence of a medial

weight shift during the last half of stance of their bipedal gait.

2. Material and methods

2.1. Materials

The modern human sample consists of adults ($n = 15$) drawing from a 20th century industrialized population housed in the Raymond A. Dart Collection of Human Skeletons at the University of the Witwatersrand, Johannesburg, South Africa (Dayal et al., 2009). In addition, Mt5s of three hunter-gatherers from Matjes River (Early/Mid Holocene) were analyzed (L'Abbe et al., 2008). These three individuals are curated by the National Museum in Bloemfontein, South Africa. Comparative samples of wild-shot, adult chimpanzees ($n = 14$) and gorillas ($n = 13$) were collected from the Department of Comparative Anatomy of the National Museum of Natural History, Paris, France and originate from Congo, Gabon and Cameroon. As with the industrialized human sample, the Mt5s from the African ape sample were taken from the same individuals whose Mt1s were previously investigated by Jashashvili and colleagues (2015).

Original *A. africanus*, *P. robustus* and *Homo* fossil hominin Mt5s in the study include: StW114/115 from Sterkfontein, Member 4 (Zipfel et al., 2009); SKX33380 from Swartkrans, Member 3 (Susman, 1989; Susman et al., 2001); UW.101-518, UW.101-1412 and UW.101-1439 from Dinaledi Chamber (Harcourt-Smith et al., 2015); OH8 from Olduvai (Day and Napier, 1964); and D4058 from Dmanisi (Lordkipanidze et al., 2007; Pontzer et al., 2010).

2.2. Computed tomography (CT) scanning protocol

The scanning protocol for the extant comparative material has been described elsewhere (Jashashvili et al., 2015). South African fossils from Sterkfontein, Swartkrans, and Dinaledi, as well as the metatarsals from Holocene human hunter-gatherers, were microCT scanned using a Nikon Metrology XTH 225/320 LC dual source industrial CT system housed in the Microfocus X-ray Computed Tomography Facility in the Evolutionary Studies Institute of the University of the Witwatersrand. The fossils were scanned at 140 kV and 140 μA energy settings using 3142 projections and a 1.2 mm copper filter. The human hunter-gatherers were scanned at 90 kV and 220 μA energy settings using 1000 projections and a 0.5 mm copper filter. All raw data were reconstructed in Inspect-X software, which is Nikon Metrology proprietary software associated with the microCT scanner. We employed a small amount of beam hardening correction (i.e. correction factor preset 2) in order to optimize image quality. Image volumes were registered as 16-bit pixel .TIF image stacks, with spatial resolutions ranging between 26 and 49 μm.

The Olduvai Mt5 was scanned at the Ocean Road Cancer Institute (Dar es Salaam, Tanzania) using a Siemens CT scanner. An EXTREMITY protocol was used for image acquisition. Relevant scan parameters for this fossil include: 120 kVp, a tube current of 67 mAs, a slice thickness of 1.0 mm, and a reconstruction increment of 0.5 mm. Subsequent to the acquisition of these raw data, image data were reconstructed as 16-bit DICOM images using a bone reconstruction algorithm (i.e. an U80u kernel value).

The Dmanisi Mt5 was scanned in the Department of Radiology at AVERSI Clinic (Tbilisi, Georgia) using a Philips Brilliance 64 medical CT scanner. The open SKULL U.H.R. 0.5 protocol (Philips Healthcare, Andover, MA, USA) was used for image acquisition. Relevant scan parameters for this fossil include: 120 kVp, a tube current of 209 mAs, a slice thickness of 0.67 mm, and a reconstruction increment of 0.3 mm. Subsequent to the acquisition of these raw data, image data were reconstructed as 16-bit DICOM images using a bone reconstruction algorithm (i.e. a "sharp" kernel).

2.3. Data collection protocol

A three-dimensional rendering for each Mt5 was produced using Avizo 9.0 software (FEI, Visualization Sciences Group), and then saved as a .STL file. Measurements were taken on left Mt5 renderings, or when absent, a right Mt5 rendering from the same individual was mirrored and used as a substitute. The initial step of the processing procedure involved reorienting each metatarsal diaphysis such that its principal longitudinal axis was parallel to the *Z*-axis, as determined by aligning landmarks positioned on the centroids of the proximal and distal articular surfaces (Fig. 1A; see also Jashashvili et al., 2015). Next, the rendering was manually rotated about the *Z*-axis (Fig. 1B) until its articular surface with the Mt4 became parallel to the *Y*-axis (as illustrated by the vertical black dashed line in Fig. 1B).

After positioning each rendering, comparable cortical thicknesses were extracted at regularly-spaced intervals (~2.94%) from 25% to 75% of diaphyseal length along the proximodistal (longitudinal) axis of the shaft (Fig. 1C and D). In all, 17 cross sections were extracted from each diaphysis, and each image within the stack of 17 contained a separate cross section that was standardized to a pixel size of 0.1 mm. Each image was saved as an 8-bit .BMP file (Fig. 1D; Jashashvili et al., 2015; see Fig. 2A).

Cortical bone thicknesses (CBTs) and second moments of area (SMAs) about *X*- (I_x) and *Y*- (I_y) neutral planes were quantified in each digital cross section appearing in the 8-bit .BMP files. Structural data were acquired from the cross sections using custom scripts in Wolfram Mathematica©10 (Wolfram Research, Inc., Mathematica, Version 10.4.1, Champaign, IL). Both CBT and SMA were calculated radially around a cross section, using one degree increments between successive measurements (Jashashvili et al., 2015; see Fig. 2 and corresponding text). All CBT measurements were scaled by biomechanical length of the metatarsal, while SMA measurements were scaled by the product of body size and bone length (Ruff, 2000; Smith and Jungers, 1997). Since the individuals in the present study were the same as those analyzed by Jashashvili and colleagues (2015), we used the same body mass estimates as were used in the earlier study of the Mt1 diaphysis. For the three additional modern human hunter-gatherers, we used the same regression formulae for estimating their body mass. Published body mass estimates were used

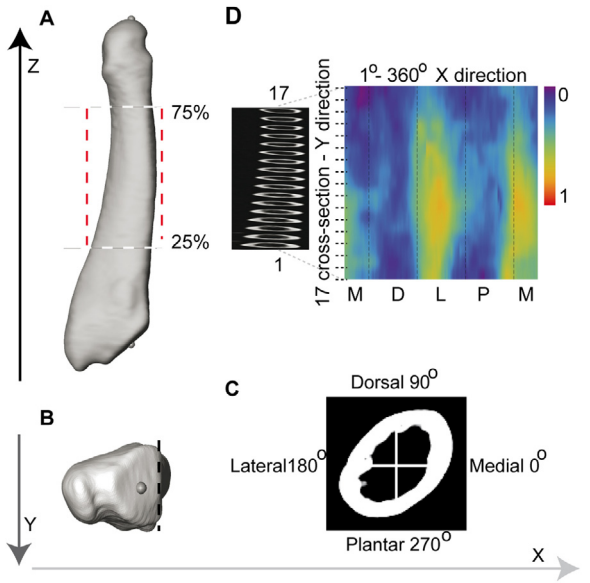

Fig. 1. Protocol for positioning a Mt5 rendering and the extraction of cross sections from its diaphysis. A: dorsal view. Landmarks positioned in centres of proximal and distal articular surfaces are used to define the longitudinal axis of a diaphysis, which subsequently is aligned to the *Z*-axis in 3D space. B: proximal view. After aligning the longitudinal axis of a rendering to the *Z*-axis in 3D space, each rendering is rotated about its longitudinal axis until the articulation for the Mt4 on the proximal articular surface (black dashed line) is parallel to the *Y*-axis. C: cross section at 50% length (between landmarks) of the rendering that is also illustrated in A. D: a total of 17 cross sections are extracted from each metatarsal in 2.94% length increments beginning at 25% (1st) and ending at 75% of diaphyseal length (17th). Cortical thicknesses in the 17 cross sections (vertical axis) are mapped to a continuous range of colours. Cortical thickness along each of the 360 rays of a cross section is visualized from left to right (horizontal axis) beginning at 0 degree (medial: M), and continuing through 90 (dorsal: D), 180 (lateral: L), and 270 degrees (plantar: P). Purple-coloured pixels (i.e. cooler colours) represent minimum thickness, while red-coloured pixels (i.e. hotter colours) represent maximum thickness.

Fig. 1. Protocole pour le positionnement 3D de la représentation surfacique d'un Mt5 et extraction des sections transversales de sa diaphyse. A : Vue dorsale. L'axe longitudinal de chaque diaphyse a été déterminé à l'aide de points repères (*landmarks*) placés aux centres des surfaces articulaires proximales et distales. Cet axe est ensuite aligné le long de l'axe *Z* dans l'espace 3D. B : Vue proximale. Après alignement de l'axe longitudinal avec l'axe *Z*, on effectue une rotation autour de l'axe longitudinal de manière à ce que l'articulation avec le Mt4 au niveau de la surface articulaire proximale (ligne noire pointillée) soit parallèle à l'axe *Y*. C : Coupe transversale à 50 % de la longueur de l'os (entre les *landmarks*). D : Au total, 17 sections sont extraites de chaque métatarse, chaque section étant séparée de la suivante en incrémentant la longueur de 2,94 % à partir de 25 % (1re section) et en terminant à 75 % de longueur diaphysaire (17e section). Les épaisseurs corticales pour les 17 sections (axe vertical) sont retranscrites en une carte de couleurs. Les variations de l'épaisseur corticale pour chacun des 360 degrés d'une section transversale donnée sont visualisées de gauche à droite (axe horizontal), en commençant à 0 degré (médiane: M) et en passant par 90 (dorsal : D), 180 (latéral: L), 270 degrés (plantaire: P). Les pixels de couleur bleu–pourpre (à savoir, les couleurs froides) représentent les épaisseurs minimales, tandis que les pixels de couleur rouge (les couleurs plus chaudes) représentent les épaisseurs maximales.

for the taxon to which each fossil has been generally attributed. For StW114/115, we used a body mass estimate reported for *A. africanus* (Grabowski et al., 2015: Table 4). For SKX33380, we used a body mass estimate reported for *P. robustus* (Grabowski et al., 2015: Table 4). Two different estimates of body mass were used for OH8: one reported for *Homo habilis* by Grabowski and colleagues (2015: Table 4), and one coinciding with the uppermost value in the range of estimated body masses for the OH8 foot (Parr et al., 2011). An estimate representing the upper end of the range reported by Parr and colleagues (rather than estimates at the lower end of the range or the middle of the range) was used so as to provide a maximal range of body mass estimates for OH8. An average estimate for Dinaledi fossils was generated by averaging all estimated body masses reported by Berger and colleagues (Berger et al., 2015). The Dmanisi metatarsal was scaled using the body mass estimate for individual II (Lordkipanidze et al., 2007).

After careful inspection of UW.101-1412 and its corresponding image data, which was originally identified as a Mt5 (Harcourt-Smith et al., 2015: SI Table 1), we chose to exclude it from our study on the grounds that this specimen, in our opinion, is a fibula shaft fragment rather than a Mt5.

2.4. Colour map visualization

The 2D colour map approach described by Jashashvili and colleagues (2015) was used to visualize morphological differences between Mt5s. Colour maps were generated using Wolfram Mathematica©10. In each colour map, the horizontal axis reflects 360 successive radii circumnavigating a cross section in one degree increments between 1 and 360 degrees. The vertical axis of each colour map reflects 17 successive cross sections proceeding from proximal to distal along a diaphysis. Colours in each map represent a third measurement, which corresponds to magnitudes of scaled structural variables (sCBT and sSMA) (Fig. 1D).

2.5. Statistical analyses

In order to evaluate group differences in sCBT and sSMA of extant taxa, a series of analysis of variance (ANOVA) tests were used. The Student–Newman–Keuls post hoc test was chosen to evaluate pairwise differences between extant taxa since this test accounts for multiple comparisons by adjusting alpha values for statistical significance. The human hunter-gatherer group ($n = 3$) was excluded from these analyses due to its small sample size.

In order to quantify the trends visualized in colour maps, a penalized discriminant analysis (PDA) was applied to sCBT and sSMA (Hastie et al., 1995; Jashashvili et al., 2015). Also, these analyses were performed in order to project fossils within the penalized discriminant function (PDF) space defined by the comparative samples. Of 42 available extant metatarsals, 36 were randomly assigned to a training sample (comprised of 12 metatarsals from each extant taxon) and six were randomly assigned to a test sample (i.e. comprised of two chimpanzees, one gorilla, and three modern humans). Penalized discriminant functions were fit to the training samples using 12-fold cross-validation in order to select the regularization parameters. Each fossil was projected in discriminant space in order to define its morphospace according to its own properties.

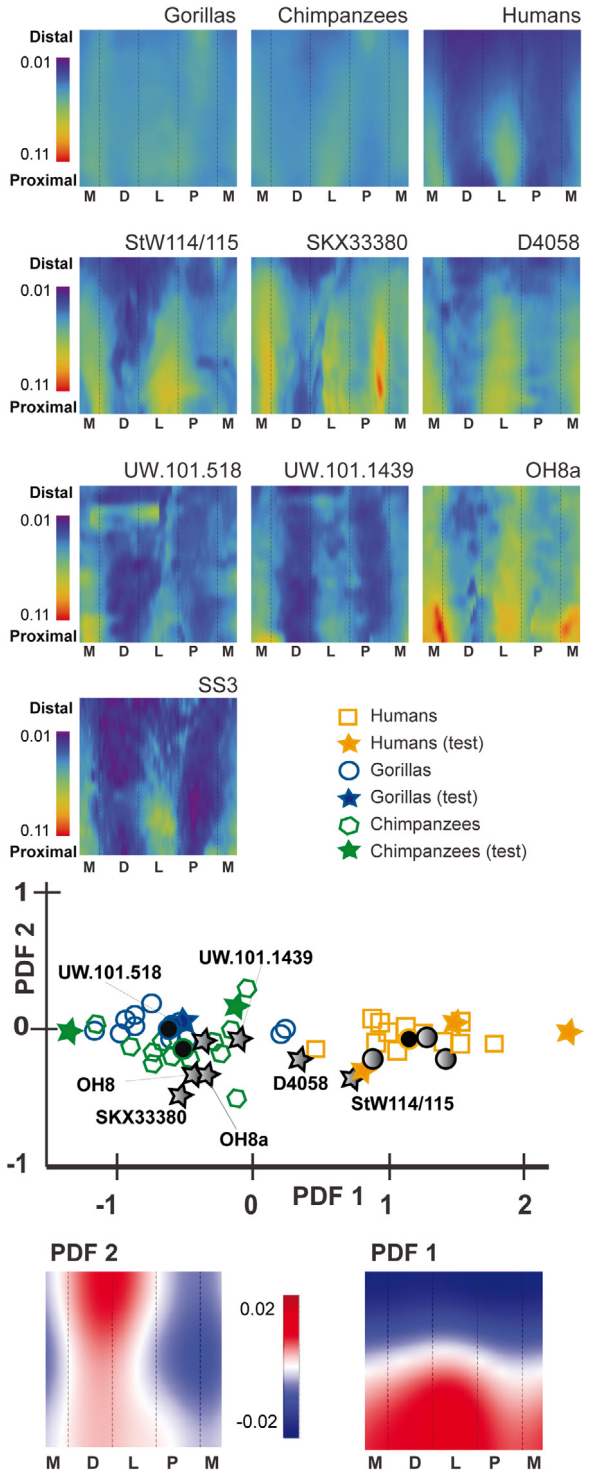

Fig. 2. Species-specific or fossil-specific distributions of scaled cortical bone thickness (sCBT) visualized with colour maps (first four rows). M: medial, D: dorsal, L: lateral, P: plantar. First row: consensus values for gorillas, chimpanzees, and modern humans. Second row: specimen values from Sterkfontein (StW114/115), Swartkrans (SKX33380), and Dmanisi (D4058). Third row: specimen values from Dinaledi (UW.101.518, UW.101.1439) and Olduvai (OH8: without correction; OH8a: with likely pathological bone on periosteal surface removed). Fourth row: specimen values from San hunter-gatherers of southern Africa from Matjes River (L'Abbe et al., 2008), with the legend for the penalized discriminant analysis (PDA) plot immediately to the right. Fifth row: plot of Penalized Discriminant Function (PDF) 1 versus PDF 2 generated from the PDA of sCBTs. The plot presents the projection of each individual Mt5 in the sample into discriminant space via PDF1 and PDF2. Black filled circles within a species cluster indicate species means in discriminant space. Open symbols in the clusters indicate subjects used in the training sample, while filled stars indicate test subjects. Grey filled stars indicate projected fossils, while grey filled circles indicate the three modern human hunter-gatherers. Sixth row: colour maps visualizing pixel-wise loadings of PDFs. Red colours correspond to positive PDF loadings across the corresponding region of a colour map. Blue colours correspond to negative PDF loadings across the corresponding region of a colour map. White colours indicate the transition between positive and negative loadings (i.e. zero loading). The aggregate of the signed loadings across a colour map produces the PDF score on a specific PDF axis for the plot above.

3. Results

3.1. Scaled cortical bone thickness (sCBT)

The modern human industrialized sample exhibited significantly lower sCBT average magnitudes than chimpanzee and gorilla samples (Table 1, Figs. 2 and 3A). The modern human hunter-gatherer sample, while slightly higher in magnitude than the industrialized sample, was qualitatively similar and thus both human groups are lumped together when interpreting colour maps because this subtle difference was not verified statistically due to the small sample size of the former. Humans exhibited much greater intra-individual variation in sCBT values compared to either African ape sample (Fig. 3A). While gorillas exhibited generally thicker sCBT than chimpanzees, these differences were not statistically significant

Fig. 2. Distributions spécifiques pour les espèces actuelles, ainsi que chez les fossiles, des épaisseurs calibrées de l'os cortical (sCBT). Ces distributions sont visualisées à l'aide de cartes de couleur (quatre premières lignes). M : Médial, D : dorsal, L : latéral, P : plantaire. Première ligne : valeurs moyennes pour les gorilles, les chimpanzés et les humains modernes. Deuxième ligne : valeurs des spécimens de Sterkfontein (StW114/115), Swartkrans (SKX33380) et Dmanisi (D4058). Troisième ligne : valeurs des spécimens de Dinaledi (UW.101.518, UW.101.1439) et d'Olduvai (OH8: sans correction; OH8a : avec enlèvement de la partie potentiellement pathologique de la surface du périoste). Quatrième ligne : valeurs des spécimens des chasseurs-cueilleurs d'Afrique du Sud de Matjes River (SS3), avec la légende des analyses discriminantes pondérées (PDA) immédiatement à droite. Cinquième ligne : premier axe discriminant pondéré (PDF 1) par rapport à PDF 2 généré par la PDA sur les valeurs de sCBT. Le graphique présente les scores de projection de chaque Mt5 de l'échantillon dans l'espace discriminant PDF1–PDF2. Les cercles noirs représentent les valeurs moyennes pour les trois espèces actuelles testées dans l'espace discriminant. Les symboles ouverts indiquent les spécimens utilisés pour construire l'espace discriminant de la PDA, tandis que les étoiles pleines représentent les sujets testés. Les étoiles grises représentent les scores de projection pour les fossiles, tandis que les cercles gris indiquent les scores de projection des humains modernes chasseurs-cueilleurs. Sixième ligne : représentation graphique des axes discriminants PDF 1 et PDF 2 en cartes de couleur. Aux couleurs rouges correspondent des valeurs positives pour les éléments constitutifs des PDFs. Les spécimens ayant les valeurs les plus élevées de sCBT dans les régions correspondantes tendent à obtenir des scores de projection positifs sur les PDF. Aux couleurs bleues correspondent des valeurs négatives pour les éléments constitutifs des PDFs. Les spécimens ayant les valeurs les plus faibles de sCBT dans les régions correspondantes tendent également à obtenir des scores de projection positifs sur les PDF. Les couleurs blanches indiquent la transition entre les espaces positifs et négatifs (à savoir, 0 indique des valeurs neutres dans le graphique ci-dessus).

Table 1
Comparisons[1] of scaled values for cortical bone thickness (sCBT).
Tableau 1
Comparaison[1] des valeurs calibrées de l'épaisseur de l'os cortical (sCBT).

	25%	35%	50%	65%	75%	All
Humans (n = 15) (industrialized)[2]	0.236 (0.057)	0.141 (0.032)	0.096 (0.021)	0.069 (0.019)	0.058 (0.018)	0.112 (0.025)
	0.152–0.358	0.100–0.203	0.069–0.130	0.050–0.116	0.038–0.103	0.080–0.159
Humans (n = 3) (hunter-gatherers)[3]	0.192 (0.055)	0.111 (0.025)	0.082 (0.014)	0.069 (0.012)	0.072 (0.021)	0.098 (0.022)
	0.128–0.224	0.083–0.131	0.067–0.093	0.056–0.080	0.048–0.085	0.073–0.111
Gorillas (n = 13)	0.072 (0.042)	0.044 (0.025)	0.037 (0.026)	0.028 (0.015)	0.028 (0.011)	0.039 (0.022)
	0.033–0.189	0.021–0.118	0.017–0.117	0.014–0.076	0.013–0.055	0.019–0.106
Chimpanzees (n = 14)	0.064 (0.020)	0.040 (0.012)	0.031 (0.008)	0.026 (0.006)	0.026 (0.006)	0.035 (0.009)
	0.038–0.099	0.026–0.063	0.021–0.047	0.018–0.039	0.019–0.035	0.024–0.051
StW114/115	0.285	0.169	0.128	0.099	0.077	0.141
	0.177–0.393	0.122–0.216	0.098–0.159	0.083–0.114	0.069–0.085	0.067–0.393
SKX33380	0.293	0.225	0.134	0.075	0.056	0.154
	0.274–0.312	0.211–0.239	0.122–0.145	0.058–0.092	0.043–0.070	0.043–0.312
D4058	0.108	0.073	0.051	0.032	0.025	0.056
	0.072–0.144	0.049–0.096	0.036–0.066	0.025–0.040	0.019–0.031	0.019–0.144
OH8 (Grabowski et al., 2015)	0.356	0.167	0.119	0.091	0.081	0.157
	0.233–0.479	0.106–0.229	0.081–0.157	0.067–0.116	0.075–0.088	0.066–0.479
OH8 (Parr et al., 2011)	0.201	0.095	0.067	0.052	0.046	0.089
	0.132–0.271	0.060–0.129	0.046–0.089	0.038–0.065	0.042–0.050	0.038–0.271
OH8a[4] (Grabowski et al., 2015)	0.303	0.167	0.119	0.091	0.081	0.150
	0.205–0.402	0.106–0.229	0.081–0.157	0.067–0.116	0.075–0.088	0.066–0.414
OH8a[4] (Parr et al., 2011)	0.172	0.095	0.067	0.052	0.046	0.085
	0.116–0.227	0.060–0.129	0.046–0.089	0.038–0.065	0.042–0.050	0.038–0.234
UW.101.518	0.081	0.050	0.035	0.035	0.033	0.045
	0.039–0.124	0.025–0.074	0.019–0.050	0.021–0.050	0.018–0.048	0.018–0.124
UW.101. 1439	0.070	0.050	0.039	0.029	0.025	0.042
	0.039–0.100	0.030–0.071	0.024–0.055	0.017–0.042	0.017–0.034	0.016–0.100
Significant comparisons[#]	H > G	H > G	H > G	H > G	H > G	H > G
	H > C	H > C	H > C	H > C	H > C	H > C

Individual values for fossils are reported as the average of the 360 radial measurements of a cross section for that individual, using the indicated position of the diaphysis (i.e. 25%, ~35%, ~50%, ~65%, and 75%). Summary statistics for individuals within the extant comparative groups are reported, where cells contain group means in the top row (and when applicable 1 s.d. for groups in parentheses), and the observed range of a group in the bottom row. H, human; G, gorilla; C, chimpanzee.

[1] ANOVA evaluating mean differences between humans (industrialized), gorillas, and chimpanzees was statistically significant ($p < 0.005$). The sample of human hunter-gatherers was not included in the ANOVA because of its small size ($n = 3$), but these individuals were included in the respective penalized discriminant analysis.

[2] Humans of different ethnic groups corresponding to the same individuals analyzed by Jashashvili and colleagues (2015), and curated in the Raymond A. Dart Collection of Human Skeletons at the University of the Witwatersrand, Johannesburg, South Africa (Dayal et al., 2009).

[3] Holocene human hunter-gatherers from Matjes River (L'Abbe et al., 2008), curated in the collections of the National Museum, Bloemfontein, South Africa.

[4] OH8a with likely pathological bone (osteophytes) digitally removed from the periosteal surface at the 25% location.

[#] Student–Newman–Keuls post hoc tests were statistically significant for the reported pairwise differences.

(Table 1, Figs. 2 and 3A). Fig. 2 illustrates extant group consensus colour maps of Mt5s, where the human sCBT pattern demonstrated: (1) thinner dorsal and plantar cortices compared to those in chimpanzee and gorilla consensus patterns, and (2) levels of thickness in the proximal half of lateral and medial cortices that were more similar to those of African apes. Humans also exhibited gradual distal tapering of medial and lateral cortical thickenings and virtually no rotation of local thickening around the diaphysis. The gorilla consensus pattern exhibited sCBT that were more transversely expansive, particularly in the proximal half of the diaphysis, than those of either chimpanzee or human consensus patterns (i.e. the medial and lateral cortical thickenings of gorillas extended transversely towards adjacent dorsal and plantar cortices to a comparatively greater extent). Otherwise, relative proximodistal similarity was exhibited along the medial and lateral cortical thickenings of chimpanzee and gorilla consensus maps. This included an external rotation of local thicknesses towards the plantar cortex in the distal diaphysis that was not observed in the human consensus map.

Scaled CBT values seldom consistently clustered fossils within extant groups in the sample (Table 1, Figs. 2 and 3A). In general, StW114/115, SKX33380, OH8, and D4058 exhibited more ape-like sCBT average magnitudes along their diaphyses (Table 1 and Fig. 3A). In contrast, UW.101-518 and UW.101-1439 exhibited more human-like sCBT average magnitudes along their diaphyses (Table 1 and Fig. 3A). With regards to the distribution of sCBT, StW114/115, OH8, and D4058 exhibited a generally similar pattern to one another, one which was definitively more human-like in terms of exhibiting local thickenings in medial and lateral cortices, but also subtly resembling ape-like structure in that these regions of local thicknesses exhibited slight external rotations in the midshaft and distal regions towards the plantar cortex (Fig. 2). However, none of these three hominin fossils exhibited the same pattern as African apes in the distribution of sCBTs in the distal diaphysis.

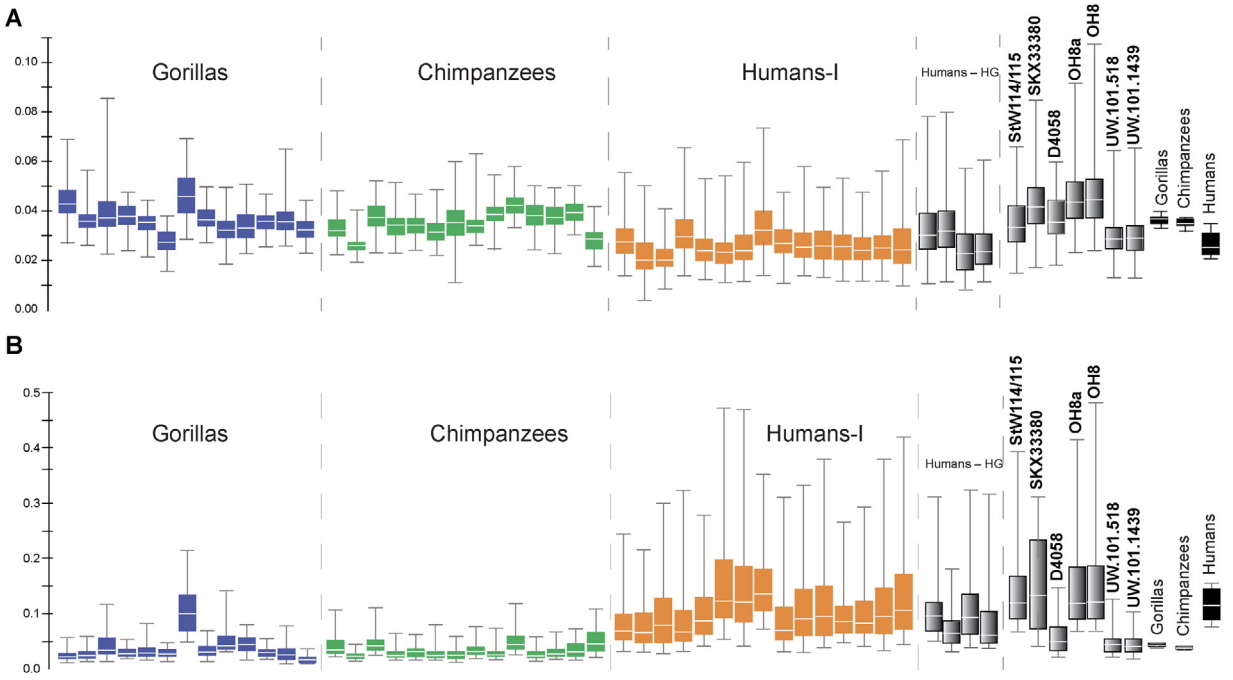

Fig. 3. A: Scaled cortical bone thicknesses in comparative and fossil Mt5s. The individual coloured boxes on the left and the middle indicate individual specific measurements (median is horizontal line, 25–75 percentile is indicated by box dimensions, and minimum and maximum values are indicated by whiskers). On the far right in grey are similarly illustrated values for additional individual Mt5s and in black are species values illustrated using the mean of each individual in the species rather than all values for an individual. Note human values reflect the industrialized sample only. B: Scaled second moments of area reported as in A. Humans-HG: Holocene humans from Matjes River; Humans-I: modern humans from an industrialized population.

Fig. 3. A : Épaisseur calibrée de l'os cortical (sCBT) des Mt5s pour l'échantillon de comparaison et chez les fossiles. Les boîtes à moustache colorées sur la gauche et au milieu indiquent les mesures pour des individus donnés (la ligne horizontale représente la médiane, la dimension de la boîte représente les 25e et 75e percentiles, les moustaches indiquent les valeurs minimales et maximales). Sur la droite du graphique, en gris, sont illustrés de façon similaire les Mt5s des fossiles. À l'extrême droite sont représentées en noir, non pas des individus, mais les valeurs moyennes pour les trois espèces de l'échantillon de comparaison. B : Les moments quadratiques ajustés (sSMA) sont représentés comme les épaisseurs corticales le sont en A. Humains-HG = échantillon holocène de Matjes River ; Humains-I = échantillon moderne d'une population industrialisée.

SKX33380 was human-like (distribution-wise) in that its highest sCBTs did not externally rotate from proximal to distal along the diaphysis, but this fossil was unique in having its highest sCBT located in the proximal half of its plantar cortex. UW.101-518 and UW.101-1439 were generally again human-like in their distributions of sCBT, except neither specimen exhibited well-defined proximal concentrations of sCBT in medial and lateral cortices, resulting in the absence of human-like distal tapering of medial and lateral cortical thickenings.

The first PDF (PDF 1) separated sCBT of modern humans (positive values) from those of chimpanzees and gorillas (negative values) (Fig. 2). Positive loading on PDF 1 reflects human differences from African apes attributable to thicker cortices in the proximal diaphysis and thinner cortices in the distal diaphysis of the former. In other words, African apes are generally more uniformly thick along the diaphysis than humans. The second PDF (PDF 2) did not clearly separate extant groups by sCBT (Fig. 2). Rather, PDF 2 appears to be driven by individual-specific variation. StW114/115 and D4058 were projected close to one another along PDF 1, and on the lower boundary of the human cluster (Fig. 2). In contrast, SK33380, OH8, UW101-518, and UW.101-1439 were firmly projected within the African ape cluster along PDF 1 (Fig. 2). Along PDF 2, SK33380 and OH8 (and to a lesser extent StW114/115 and D4058) were projected on the (lower) margin of the entire extant sample cluster, while UW.101-518 and UW.101-1439 were firmly projected within the entire extant sample cluster (Fig. 2).

3.2. Scaled second moments of area (sSMA)

The modern human industrialized sample exhibited significantly higher sSMA average magnitudes than chimpanzee and gorilla samples (Table 2, Figs. 3B and 4). The modern human hunter-gatherer sample, while generally slightly lower in magnitude than the human industrialized sample, was qualitatively similar and thus both human groups are again lumped together when interpreting colour maps because this subtle difference was not verified statistically due to the small sample size of the former. Humans exhibited much greater intra-individual variation in sSMA values compared to either African ape sample (Fig. 3B). While gorillas exhibited generally higher sSMAs than chimpanzees, these differences were not statistically significant (Table 2, Figs. 3B and 4). Fig. 4 illustrates extant group consensus colour maps of Mt5s, where the human sSMA pattern demonstrated absolutely more diaphyseal rigidity compared to chimpanzee and gorilla consensus patterns,

Table 2
Comparisons[1] of scaled values for second moments of area (sSMA).
Tableau 2
Comparaison[1] des valeurs calibrées pour les moments quadratiques (sSMA).

	25%	35%	50%	65%	75%	All
Humans ($n = 15$) (industrialized[2]	0.236 (0.057)	0.141 (0.032)	0.096 (0.021)	0.069 (0.019)	0.058 (0.018)	0.112 (0.025)
	0.152–0.358	0.100–0.203	0.069–0.130	0.050–0.116	0.038–0.103	0.080–0.159
Humans ($n = 3$) (hunter-gatherers)[3]	0.192 (0.055)	0.111 (0.025)	0.082 (0.014)	0.069 (0.012)	0.072 (0.021)	0.098 (0.022)
	0.128–0.224	0.083–0.131	0.067–0.093	0.056–0.080	0.048–0.085	0.073–0.111
Gorillas ($n = 13$)	0.072 (0.042)	0.044 (0.025)	0.037 (0.026)	0.028 (0.015)	0.028 (0.011)	0.039 (0.022)
	0.033–0.189	0.021–0.118	0.017–0.117	0.014–0.076	0.013–0.055	0.019–0.106
Chimpanzees ($n = 14$)	0.064 (0.020)	0.040 (0.012)	0.031 (0.008)	0.026 (0.006)	0.026 (0.006)	0.035 (0.009)
	0.038–0.099	0.026–0.063	0.021–0.047	0.018–0.039	0.019–0.035	0.024–0.051
StW114/115	0.285	0.169	0.128	0.099	0.077	0.141
	0.177–0.393	0.122–0.216	0.098–0.159	0.083–0.114	0.069–0.085	0.067–0.393
SKX33380	0.293	0.225	0.134	0.075	0.056	0.154
	0.274–0.312	0.211–0.239	0.122–0.145	0.058–0.092	0.043–0.070	0.043–0.312
D4058	0.108	0.073	0.051	0.032	0.025	0.056
	0.072–0.144	0.049–0.096	0.036–0.066	0.025–0.040	0.019–0.031	0.019–0.144
OH8 (Grabowski et al., 2015)	0.356	0.167	0.119	0.091	0.081	0.157
	0.233–0.479	0.106–0.229	0.081–0.157	0.067–0.116	0.075–0.088	0.066–0.479
OH8 (Parr et al., 2011)	0.201	0.095	0.067	0.052	0.046	0.089
	0.132–0.271	0.060–0.129	0.046–0.089	0.038–0.065	0.042–0.050	0.038–0.271
OH8a[4] (Grabowski et al., 2015)	0.303	0.167	0.119	0.091	0.081	0.150
	0.205–0.402	0.106–0.229	0.081–0.157	0.067–0.116	0.075–0.088	0.066–0.414
OH8a[4] (Parr et al., 2011)	0.172	0.095	0.067	0.052	0.046	0.085
	0.116–0.227	0.060–0.129	0.046–0.089	0.038–0.065	0.042–0.050	0.038–0.234
UW.101.518	0.081	0.050	0.035	0.035	0.033	0.045
	0.039–0.124	0.025–0.074	0.019–0.050	0.021–0.050	0.018–0.048	0.018–0.124
UW.101. 1439	0.070	0.050	0.039	0.029	0.025	0.042
	0.039–0.100	0.030–0.071	0.024–0.055	0.017–0.042	0.017–0.034	0.016–0.100
Significant comparisons[#]	*Homo* > *Gorilla*	*Homo* > *Gorilla*	*Homo* > *Gorilla*	*Homo* > *Gorilla*	*Homo* > *Gorilla*	*Homo* > *Gorilla*
	Homo > *Pan*	*Homo* > *Pan*	*Homo* > *Pan*	*Homo* > *Pan*	*Homo* > *Pan*	*Homo* > *Pan*

Individual values for fossils are reported as the average of the 360 measurements of a cross section for that individual, using the indicated position of the diaphysis (i.e. 25%, ~35%, ~50%, ~65%, and 75%). Summary statistics for individuals within the extant comparative groups are reported, where cells contain group means in the top row (and when applicable 1 s.d. for groups in parentheses), and the observed range of a group in the bottom row. H, human; G, gorilla; C, chimpanzee.

[1] ANOVA evaluating mean differences between humans (industrialized), gorillas, and chimpanzees was statistically significant ($p < 0.005$). The sample of human hunter-gatherers was not included in the ANOVA because of its small size ($n = 3$), but these individuals were included in the respective penalized discriminant analysis.

[2] Humans of different ethnic groups corresponding to the same individuals analyzed by Jashashvili and colleagues (2015), and curated in the Raymond A. Dart Collection of Human Skeletons at the University of the Witwatersrand, Johannesburg, South Africa (Dayal et al., 2009).

[3] Holocene human hunter-gatherers from Matjes River (L'Abbe et al., 2008), curated in the collections of the National Museum, Bloemfontein, South Africa.

[4] OH8 with likely pathological bone (osteophytes) digitally removed from the periosteal surface at the 25% location.

[#] Student–Newman–Keuls post hoc tests were statistically significant for the reported pairwise differences.

although this difference was most starkly expressed in dorsal and plantar cortices of the proximal half of diaphyses. A clear pattern of distal attenuation in rigidity was evident in dorsal and plantar cortices of the human Mt5 consensus map.

Scaled SMA values occasionally clustered fossils with extant groups in the sample (Table 2, Figs. 3B and 4). StW114/115, SKX33380, and OH8 exhibited relatively human-like average magnitudes of sSMAs along their diaphyses, while D4058, UW.101-518, and UW.101-1439 exhibited more African ape-like average magnitudes of sSMAs along their diaphyses (Table 2, Fig. 3B). With regards to the distribution of sSMA, StW114/115 and OH8, and to a lesser extent SKX33380, again exhibited generally similar (and human-like) patterns of rigidity along diaphyses where dorsal and plantar cortices exhibited markedly greater rigidity than medial and lateral cortices (Fig. 4). While D4058, UW.101-518, and UW.101-1439 also exhibited these patterns in the distribution of sSMA, their overall rigidity was globally reduced compared to StW114/115, SKX33380, OH8, and humans, nor did they exhibit the same extent of marked differences between dorsal and plantar cortices on the one hand and medial and lateral cortices on the other. Interestingly, the subtle external rotation of highest rigidity in the distal diaphysis that was observed in the small human hunter-gatherer sample was not apparent in any of the fossil Mt5s.

The first penalized discriminant function (PDF 1) separated sSMA of modern humans (positive values) from those of chimpanzees and gorillas (negative values) (Fig. 4). Positive loading on PDF 1 reflects human differences from African apes attributable to more rigidity in dorsal and plantar cortices in the proximal, and to a lesser extent the distal, region of the metatarsal diaphysis of the former. While PDF 2 did not cleanly separate any of the extant groups, slight separation between chimpanzees and gorillas occurred. Again, PDF 2 appears to be more driven by individual-specific variation. StW114/115 and SK33380 were projected firmly within the human cluster along PDF 1, while OH8 was projected on the boundary of

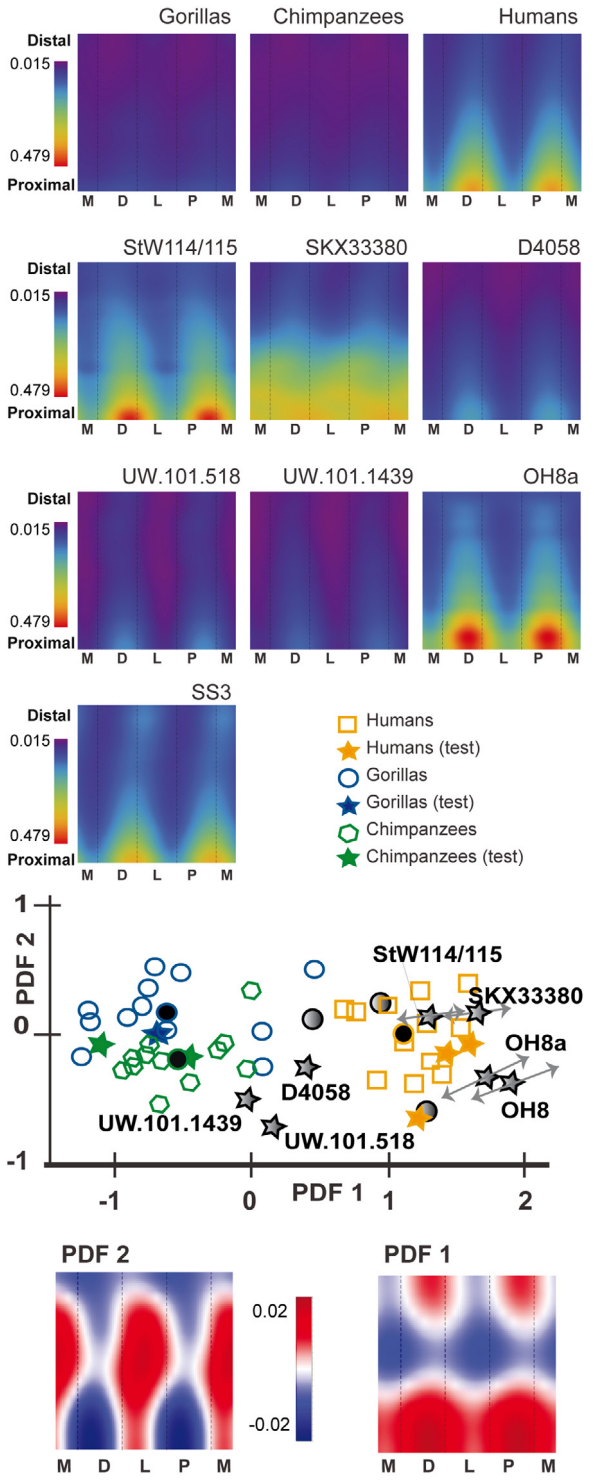

Fig. 4. Species-specific or fossil-specific distributions of scaled second moments of area (sSMA) visualized with colour maps (first four rows). M: Medial, D: dorsal, L: lateral, P: plantar. First row: consensus values for gorillas, chimpanzees, and modern humans. Second row: specimen values from Sterkfontein (StW114/115), Swartkrans (SKX33380), and Dmanisi (D4058). Third row: specimen values from Dinaledi (UW.101.518, UW.101.1439) and Olduvai (OH8: without correction; OH8a: with likely pathological bone on periosteal surface removed). Fourth row: specimen values from San hunter-gatherers of southern Africa from Matjes River (SS3), with the legend for the penalized discriminant analysis (PDA) plot immediately to the right. Fifth row: plot of Penalized Discriminant Function (PDF) 1 versus PDF 2 generated from the PDA of sSMAs. The plot presents the projection of each individual Mt5 in the sample into discriminant space via PDF1 and PDF2. Black filled circles within a species cluster indicate species means in discriminant space. Open symbols indicate subjects used in the training sample, while filled stars indicate test subjects. Grey filled stars indicate projected fossils, where grey arrows extending from fossils indicate a range of sSMAs using different scaling factors that reflect a published range of associated body mass estimates (see Section 2 for additional information). Grey filled circles indicate modern human hunter-gatherers. Sixth row: colour maps visualizing pixel-wise loadings of PDFs. Red colours correspond to positive PDF loadings across the corresponding region of a colour map. Blue colours correspond to negative PDF loadings across the corresponding region of a colour map. White colours indicate the transition between positive and negative loadings (i.e. zero loading). The aggregate of the signed loadings across a colour map produces the PDF score on a specific PDF axis for the plot above.

the human cluster opposite from the African ape cluster. By comparison, D4058, UW.101-518, and UW.101-1439 were projected just outside the boundary of the human cluster, and on the margin of the African ape cluster (i.e. in a relatively intermediate position). Along PDF 2, StW114/115, SKX33380, and D4058 were projected within the entire extant sample cluster, while OH8, UW.101.518, and UW.101.1439 were projected on the (lower) margin of the entire extant sample cluster.

4. Discussion

In this study we investigated internal structure of the Mt5 diaphysis in order to better understand how modern humans, African apes, and fossil hominins load

Fig. 4. Distributions spécifiques pour les espèces actuelles, ainsi que chez les fossiles, des moments quadratiques ajustés (sSMA). Ces distributions sont visualisées à l'aide de cartes de couleur (quatre premières lignes). M : Médial, D : dorsal: L : latéral, P : plantaire. Première ligne : valeurs moyennes pour les gorilles, les chimpanzés et les humains modernes. Deuxième ligne : valeurs des spécimens de Sterkfontein (StW114/115), Swartkrans (SKX33380) et Dmanisi (D4058). Troisième ligne : valeurs des spécimens de Dinaledi (UW.101.518, UW.101.1439) et d'Olduvai (OH8 : sans correction ; OH8a : avec enlèvement de la partie potentiellement pathologique de la surface du périoste). Quatrième ligne: valeurs des spécimens des chasseurs-cueilleurs d'Afrique du Sud de Matjes River (SS3), avec la légende des analyses discriminantes pondérées (PDA) immédiatement à droite. Cinquième ligne: premier axe discriminant pondéré (PDF 1) par rapport à PDF2 généré par la PDA sur les valeurs de sSMA. Le graphique présente les scores de projection de chaque cinquième métatarsien de l'échantillon dans l'espace discriminant PDF1–PDF2. Les cercles noirs représentent les valeurs moyennes pour les trois espèces actuelles testées dans l'espace discriminant. Les symboles ouverts indiquent les spécimens utilisés pour construire l'espace discriminant de la PDA, tandis que les étoiles noires représentent les sujets testés. Les étoiles grises représentent les scores de projection pour les fossiles, tandis que les cercles gris indiquent les scores de projection des humains modernes chasseurs-cueilleurs. Sixième ligne : représentation graphique des axes discriminants PDF 1 et PDF 2 en cartes de couleur. Aux couleurs rouges correspondent des valeurs positives pour les éléments constitutifs des PDFs. Les spécimens ayant les valeurs les plus élevées de sSMA dans les régions correspondantes tendent à obtenir des scores de projection positifs sur les PDF. Aux couleurs bleues correspondent des valeurs négatives pour les éléments constitutifs des PDFs. Les spécimens ayant les valeurs les plus faibles de sSMA dans les régions correspondantes tendent également à obtenir des scores de projection positifs sur les PDFs. Les couleurs blanches indiquent la transition entre les espaces positifs et négatifs (à savoir, 0 indique des valeurs neutres dans le graphique ci-dessus).

their feet during gait. Using a 'whole shaft' approach, we visualized and quantified differences in two Mt5 structural parameters – cortical bone thickness and second moments of area – that previously differentiated modern human and African ape Mt1 structure in accordance with predictions based on their foot loading regimes (Jashashvili et al., 2015). As predicted, the human Mt5 diaphysis exhibited preferential reinforcement for resisting dorsoplantar loading compared to Mt5 diaphyses of chimpanzees or gorillas. A similar emphasis on dorsoplantar reinforcement was observed in the human Mt1 (Jashashvili et al., 2015). Dorsoplantar reinforcement in human Mt5s was concentrated in the proximal half of the diaphysis (Fig. 4), which coincides with the location of theoretical peak principle stresses in a finite element model of the human Mt5 diaphysis (Arangio et al., 1997). The observed human pattern was not consistent with the theoretical model of Preuschoft (1969) who suggested that mediolateral directed bending moments in the Mt5 of modern humans should be higher relative to dorsoplantar directed bending moments. In balancing an adaptive trade-off between maintaining sufficient bone strength and minimizing distal mass, a proximal concentration of cortical thickness (i.e. mass) and robusticity in the lower limb of humans has been suggested as an effective strategy for optimizing energetic costs during bipedal walking (Shaw et al., 2014; Stock, 2006). Based on our analyses of the human Mt5 diaphysis (Fig. 2), such an adaptive solution may occur not only within the lower limb overall, but also possibly on a more local scale (i.e. within segmental elements such as a metatarsal and thus within the load arm of the foot). Additionally, dorsoplantar reinforcement of human Mt5s was accomplished largely by an expanded dorsoplantar external dimension of the entire diaphysis as opposed to thickening dorsal and plantar cortices (i.e. perhaps also signalling selection for tissue economy) since medial and lateral cortices of human Mt5s actually exhibited comparatively greater thicknesses (Figs. 2 and 3A). Interestingly, a similar emphasis on proximal concentration of cortical thickness in the human Mt1 diaphysis (i.e. distal tapering), by comparison, was not observed (Jashashvili et al., 2015).

Chimpanzees and gorillas similarly exhibited Mt5 diaphyses with comparatively more uniform cortical thickness (Fig. 2) and second moments of area (Fig. 4) both radially around and longitudinally along their diaphyses. The observed ape pattern was consistent with the theoretical model of Preuschoft (1969) who predicted relatively equivalent dorsoplantar and mediolateral directed bending moments in their Mt5 diaphyses. This pattern is fundamentally different from the pattern exhibited in modern humans. Such a stark contrast in patterns was not as apparent in Mt1 diaphyses of these groups (Jashashvili et al., 2015). The African ape pattern observed in the present study is consistent with a metatarsus reinforced against more varied loading compared to the human pattern that is consistent with a metatarsus reinforced against relatively stereotypical dorsoplantar loading. Interestingly, the consensus pattern of the human industrialized sample did not exhibit external rotation in the orientation of highest rigidity proximodistally along the diaphysis, but there appears to be a subtle external rotation exhibited proximodistally along the diaphysis in the consensus pattern of the small sample of human hunter-gatherers. Specifically in the latter, dorsal and plantar cortices exhibited the highest rigidity in the proximal half of the diaphysis, while approximately at midshaft the orientation of highest rigidity externally rotated towards the medial and lateral cortices through the distal half of the diaphysis. While a larger sample of human hunter-gatherers is needed to confirm whether potential differences from the industrialized humans are representative or idiosyncratic, it is interesting to consider that compared to level substrates, uneven substrates have been shown to elicit more variable step lengths and step widths in bipedal humans (Voloshina and Ferris, 2015; Voloshina et al., 2013), which presumably induces more variable contacts between the foot and substrate (i.e. foot loading patterns).

The absence of human-like distal tapering in the African ape Mt5 diaphysis also is consistent with a scenario of more varied loading in which there would appear to be relatively weaker selective pressure for minimizing distal mass distribution compared to relatively stronger selective pressure for maintaining adequate bone strength along the entire diaphysis. Ultimately, more varied loading experienced by African ape Mt5s may be the result of their relatively greater locomotor diversity and substrate use (Gebo, 1992), as well as retaining a grasping foot. It is worth noting that while magnitudes of sCBT and sSMA did not differentiate chimpanzee from gorilla Mt5 diaphyses (Table 1, Fig. 3), distributions of sCBT did. Specifically, gorillas exhibited slightly more transversely extended thickenings than chimpanzees (Fig. 2). Thus, the 'whole shaft' approach adopted here offers additional, richer insights into hominoid metatarsal structure that traditionally limited comparisons of single cross-sectional regions of interest (e.g., Marchi, 2005) or robusticity indices (Day and Napier, 1964; Harcourt-Smith et al., 2015; Pontzer et al., 2010; Zipfel et al., 2009) cannot.

Internal structure of fossil hominin Mt5 diaphyses was not consistent across the sample, suggesting that systemic skeletal gracilization and loading patterns of the lateral column of the foot appear to have differed amongst these hominins. Diaphyses of Mt5s from *A. africanus* (StW114/115), *P. robustus* (SKX33380), *H. habilis* (OH8), and *H. erectus* (D4058) exhibited African ape-like levels of cortical thickness, whereas only *H. naledi* Mt5s (UW.101-518 and UW.101-1439) exhibited human-like levels of cortical thickness (Table 1 and Fig. 3A). Of the fossil Mt5s included in the present analysis, only *A. africanus* (StW114/115) and *H. erectus* (D4058) Mt5s exhibited the unique human-like distal tapering in cortical thickness observed here (Fig. 2). Postcranial gracilization is thought to be a relatively recent phenomenon within human evolution (i.e. emerging within the Holocene), as demonstrated by temporal trends in trabecular (Chirchir et al., 2015; Ryan and Shaw, 2015) and cortical bone decreases (Ruff et al., 1993; Shaw and Stock, 2013; Stock, 2006). Explanations for skeletal gracilization abound, ranging from reduced activity levels associated with increased sedentariness, dietary shifts, and hormonal changes, among others (Carlson and Marchi, 2014b). While dates for *H. naledi* fossils have not yet been assigned (Harcourt-Smith et al., 2015),

their generally human-like cortical thinning is suggestive evidence that skeletal gracilization may characterize *H. naledi*. Reasons for this are unknown; moreover, systematic sampling of other anatomical regions of the *H. naledi* postcranial skeleton must be undertaken before this trend can be confirmed. Neither of the two *H. naledi* Mt5 specimens examined in the study exhibited human-like distal tapering in cortical thickness (i.e. optimization in mass distribution), but both were similar to other fossil (e.g., OH8 and SKX33380), chimpanzee, and gorilla Mt5s in exhibiting continuations of thickened regions into distal halves of diaphyses (Fig. 2). This implies that selective pressures on metatarsal structure experienced by these hominins (e.g., gait kinematics) probably differed from those experienced by modern humans investigated in the present study, corroborating the few primitive foot morphological characters that were reported (Harcourt-Smith et al., 2015).

Diaphyses of *A. africanus* (StW114/115), *P. robustus* (SKX33380), and *H. habilis* (OH8) Mt5s combined ape-like magnitudes of cortical thickness and human-like magnitudes of rigidity. This is consistent with diaphyseal reinforcement via cortical thickening rather than increasing dorsoplantar external dimensions, although the degree of intra-individual variation in both variables exhibited by these fossils (Fig. 3) suggests that to some extent they combined both functional solutions for enhancing dorsoplantar diaphyseal rigidity. It also supports previous suggestions of human-like loading in the lateral column of the foot of these hominins (Day and Napier, 1964; Proctor, 2013; Zipfel et al., 2009). The *H. erectus* Mt5 from Dmanisi (D4058) uniquely combined ape-like magnitudes of cortical thickness and rigidity (Fig. 3). This is consistent with other primitive retentions noted in the metatarsals of the hominins from Dmanisi (Pontzer et al., 2010), and also with the lack of a relatively human-like expanded Mt5 dorsoplantar external dimension (e.g., robusticity index). Both of these results suggest that human-like selective pressures on the foot (i.e. gait kinematics) may not have fully emerged in *H. erectus* from Dmanisi, echoing the assessment of others (Pontzer et al., 2010). In contrast, *H. naledi* (UW.101-518 and UW.101-1439) Mt5s were unusual amongst the hominin sample in that they coupled human-like magnitudes of cortical thickness and ape-like magnitudes of rigidity (Tables 1 and 2, Fig. 3). This suggests that *H. naledi* Mt5s were relatively gracile (human-like), but also less rigid (i.e. loaded) than those of other hominin taxa investigated in the study. Importantly, the Mt5s of *H. naledi* were not particularly human-like in that they did not exhibit distal tapering in cortical thickness. Functional interpretation of the observed *H. naledi* uniqueness amongst the hominin sample in this study requires further comparative investigations of *H. naledi* postcrania.

Similar sSMA distributions defined a group formed by StW114/115 and OH8, and to a lesser extent SKX33380 (i.e. emphasis on human-like dorsoplantar rigidity in the proximal half of the diaphysis), as well as a second group formed by D4058, UW.101-518, and UW.101-1439 (i.e. relative emphasis on ape-like invariable rigidity radially around and longitudinally along the diaphysis) (Fig. 4). Contrary to our prediction, the *A. africanus* Mt5 (StW114/115) was not more ape-like in internal structure than the *H. habilis* Mt5 (OH8), which supports the notion of (functional) conservatism within the lateral column of the hominin foot. However, the internal structural variability in Mt5s observed amongst all fossil hominins investigated in the study clearly argues against (functional) conservatism in the lateral column of the hominin foot, contra suggestions made from comparisons of external structure (Harcourt-Smith et al., 2015; Proctor, 2013; Ward et al., 2011). Moreover, other *Homo* Mt5s besides that of OH8, specifically those from *H. erectus* (D4058) and *H. naledi* (UW.101-518 and UW.101-1439), were unexpectedly more African ape-like in some aspects of their internal structure than was the *A. africanus* Mt5 (StW114/115). This suggests that despite what appears to be conserved external morphological features in the hominin lateral column of the foot (Harcourt-Smith et al., 2015; Proctor, 2013; Ward et al., 2011), the loading patterns sustained by the lateral column still varied within these hominins, particularly distinguishing *H. erectus* from Dmanisi and *H. naledi* from Dinaledi for different reasons. The observed relatively ape-like features in the internal structure of the Dmanisi Mt5 (D4058) are particularly surprising given that other lower limb adaptations in the Dmanisi postcranium have been suggested to evince strong selection for efficient bipedal gait (Pontzer et al., 2010). We reiterate what others have suggested (Hatala et al., 2016; Rose, 1991), namely, that the evolution of human bipedalism was a process that involved a number of hominins characterized by a number of experiments in gait kinematics (and thus loading patterns) along the way.

There can be no doubt that the kinematics and loads sustained by the foot during locomotor repertoires are complicated. For example, *in vivo* experimental studies using motion capture systems, force transducers, and dynamic pressure sensors continue to demonstrate the importance of intra- and inter-individual variation in both modern humans and chimpanzees/bonobos (e.g., Bates et al., 2013; D'Août et al., 2004; De Cock et al., 2008; Fernández et al., 2016; Vereecke et al., 2003). Unfortunately, fewer data exist for gorillas (but see Schmitt et al., 2016). Some of the observed variations can be due to general effects on gait of speed, foot and lower limb pathologies, body size, and/or substrate preferences, etc. (Carlson and Demes, 2010; Franz et al., 2005; Schmitt, 2003; Schmitt and Hanna, 2004). Despite this potential for load variation in and between humans and apes, the internal structure of the Mt1 (Jashashvili et al., 2015; Marchi, 2005) and Mt5 (this study; Marchi, 2005) is consistently informing us that there is a significant difference between humans and apes. The fact that fossil hominins are variable, and appear to be bracketed by these extant hominid groups, at least for the Mt5 diaphysis, highlights the fact that the internal morphology of the lateral column of their foot has not uniformly converged on a stereotypical modern human pattern, and by extension, that their foot biomechanics (especially in the lateral column) are equally not necessarily like that of modern humans. Future investigations that would include Mt5s from additional Plio-Pleistocene fossil hominins, including Neanderthals, would further evaluate this hypothesis by more comprehensively assessing when modern human internal morphology first appeared

in the human evolutionary record. Additionally, applying the "whole shaft" approach to other metatarsals of fossil hominins, such as the Mt1, would appear to be equally promising for understanding the evolution of modern human foot form and function.

Author contributions

Conceived and designed the experiments: TJ, MRD, KJC, and RL; performed the experiments (acquired X-ray data): TJ, RL, and RLS; analyzed the data: MRD, TJ, KJC, and RL; contributed to the writing of the manuscript: TJ, KJC, MRD, RL, BAP, RLS, and DL.

Funding

PAST – Palaeontological Scientific Trust. The South African Department of Science and Technology and the National Research Foundation (South Africa), as well as the Centre of Excellence in Palaeosciences and the Evolutionary Studies Institute at the University of the Witwatersrand, provided funding in support of the Virtual Imaging in Palaeosciences (VIP) laboratory where these analyses were performed. The L.S.B. Leakey Foundation to RLS. The funders had no role in the study design, data collection and analysis, decision to publish, or preparation of the manuscript.

Acknowledgments

We would like to thank the co-editors of this special volume, Roberto Macchiarelli and Clément Zanolli, for the invitation to contribute to it. We also would like to acknowledge the inspiration provided by Laurent Puymerail in our pursuit of this approach. We thank Miss S. Potze for support and access during data collection at the Ditsong (formerly Transvaal) National Museum of Natural History in Pretoria, South Africa. We thank Dr. B. Zipfel for support and access during data collection at the Evolutionary Studies Institute, University of the Witwatersrand, South Africa. We thank Prof. J. Brink for support and access during data collection at the National Museum in Bloemfontein, South Africa. We thank Dr. Ch. Lefèvre for support and access during data collection in Paris. We thank Mr. B. Billings for support and access during data collection in Johannesburg. We thank Prof. P. Grenier and Mrs. B. Begenau (Hôpital Pitié-Salpêtrière, Paris) for permitting access to CT facilities. We thank the Evolutionary Studies Institute, the University of the Witwatersrand's Microfocus X-ray Computed Tomography Facility (https://www.wits.ac.za/microct/) for access to high resolution CT facilities. We thank Mrs. J. Smilg and Mrs. Q. Letsoalo for assistance in the CT facilities of Charlotte Maxeke Johannesburg Academic Hospital. We thank Dr. N. Sainishvili (AVERSI Clinic Tbilisi, Georgia) for permitting access to CT facilities. We thank Dr. H. Said Myanza for assistance in the CT facilities of the Ocean Road Cancer Institute, Dar-es-Salaam, Tanzania. Finally, we also thank the Virtual Imaging in Palaeosciences (VIP) laboratory, Evolutionary Studies Institute (ESI) at the University of the Witwatersrand.

References

Arangio, G.A., Xiao, D., Salathe, E.P., 1997. Biomechanical study of stress in the fifth metatarsal. Clin. Biomech. 12, 160–164.

Archibald, J.D., Lovejoy, C.O., Heiple, K.G., 1972. Implications of relative robusticity in the *Olduvai metatarsus*. Am. J. Phys. Anthropol. 37, 93–95.

Bates, K.T., Collins, D., Savage, R., McClymont, J., Webster, E., Pataky, T.C., D'Aout, K., Sellers, W.I., Bennett, M.R., Crompton, R.H., 2013. The evolution of compliance in the human lateral mid-foot. Proc. Biol. Sci. 280, 20131818, http://dx.doi.org/10.1098/rspb.2013.1818.

Berger, L.R., Hawks, J., de Ruiter, D.J., Churchill, S.E., Schmid, P., Delezene, L.K., Kivell, T.L., Garvin, H.M., Williams, S.A., DeSilva, J.M., Skinner, M.M., Musiba, C.M., Cameron, N., Holliday, T.W., Harcourt-Smith, W., Ackermann, R.R., Bastir, M., Bogin, B., Bolter, D., Brophy, J., Cofran, Z.D., Congdon, K.A., Deane, A.S., Dembo, M., Drapeau, M., Elliott, M.C., Feuerriegel, E.M., Garcia-Martinez, D., Green, D.J., Gurtov, A., Irish, J.D., Kruger, A., Laird, M.F., Marchi, D., Meyer, M.R., Nalla, S., Negash, E.W., Orr, C.M., Radovcic, D., Schroeder, L., Scott, J.E., Throckmorton, Z., Tocheri, M.W., VanSickle, C., Walker, C.S., Wei, P., Zipfel, B., 2015. *Homo naledi*, a new species of the genus *Homo* from the Dinaledi Chamber, South Africa. Elife 4, e09560.

Bojsen-Møller, F., 1979. Calcaneocuboid joint and stability of the longitudinal arch of the foot at high and low gear push off. J. Anat. 129, 165–176.

Carlson, K.J., Demes, B., 2010. Gait dynamics of *Cebus apella* during quadrupedalism on different substrates. Am. J. Phys. Anthropol. 142, 273–286.

Carlson, K.J., Marchi, D., 2014a. Introduction: towards refining the concept of mobility. In: Carlson, K.J., Marchi, D. (Eds.), Reconstructing Mobility – Environmental, Behavioral, and Morphological Determinants. Springer, New York, pp. 1–11.

Carlson, K.J., Marchi, D.M. (Eds.), 2014b. Reconstructing Mobility – Environmental, Behavioral, and Morphological Determinants. Springer, New York.

Chirchir, H., Kivell, T.L., Ruff, C.B., Hublin, J.-J., Carlson, K.J., Zipfel, B., Richmond, B.G., 2015. Recent origin of low trabecular bone density in modern humans. Proc. Natl. Acad. Sci. U.S.A. 112, 366–371.

Crompton, R.H., Pataky, T.C., Savage, R., D'Aout, K., Bennett, M.R., Day, M.H., Bates, K., Morse, S., Sellers, W.I., 2012. Human-like external function of the foot, and fully upright gait, confirmed in the 3.66 million year old Laetoli hominin footprints by topographic statistics, experimental footprint-formation and computer simulation. J. Roy. Soc. Interface 9, 707–719.

D'Août, K., Pataky, T.C., De Clercq, D., Aerts, P., 2009. The effects of habitual footwear use: foot shape and function in native barefoot walkers. Footwear Sci. 1, 81–94.

D'Août, K., Vereecke, E., Schoonaert, K., De Clercq, D., Van Elsacker, L., Aerts, P., 2004. Locomotion in bonobos (*Pan paniscus*): differences and similarities between bipedal and quadrupedal terrestrial walking, and a comparison with other locomotor modes. J. Anat. 104, 353–361.

Day, M.H., Napier, J.R., 1964. Fossil foot bones. Nature 201, 969–970.

Dayal, M.R., Kegley, A.D., Strkalj, G., Bidmos, M.A., Kuykendall, K.L., 2009. The history and composition of the Raymond A. Dart Collection of Human Skeletons at the University of the Witwatersrand, Johannesburg, South Africa. Am. J. Phys. Anthropol. 140, 324–335.

De Cock, A., Vanrenterghem, J., Willems, T., Witvrouw, E., De Clercq, D., 2008. The trajectory of the centre of pressure during barefoot running as a potential measure of foot function. Gait Posture 27, 669–675.

DeSilva, J.M., 2010. Revisiting the "midtarsal break". Am. J. Phys. Anthropol. 141, 245–258.

DeSilva, J.M., Gill, S.V., 2013. Brief communication. A midtarsal (midfoot) break in the human foot. Am. J. Phys. Anthropol. 151, 495–499.

DeSilva, J.M., Bonne-Annee, R., Swanson, Z., Gill, C.M., Sobel, M., Uy, J., Gill, S.V., 2015. Midtarsal break variation in modern humans: functional causes, skeletal correlates, and paleontological implications. Am. J. Phys. Anthropol. 156, 543–552.

DeSilva, J.M., Holt, K.G., Churchill, S.E., Carlson, K.J., Walker, C.S., Zipfel, B., Berger, L.R., 2013. The lower limb and mechanics of walking in *Australopithecus sediba*. Science 340, 1232999, http://dx.doi.org/10.1126/science.1232999.

Drapeau, M.S.M., Harmon, E.H., 2013. Metatarsal torsion in monkeys, apes, humans and australopiths. J. Hum. Evol. 64, 93–108.

Elftman, H., Manter, J., 1935a. Chimpanzee and human feet in bipedal walking. Am. J. Phys. Anthropol. 20, 69–79.

Elftman, H., Manter, J., 1935b. The evolution of the human foot, with especial reference to the joints. J. Anat. 70, 56–67.

Fernández, P.J., Almécija, S., Patel, B.A., Orr, C.M., Tocheri, M.W., Jungers, W.L., 2015. Functional aspects of metatarsal head shape in humans, apes, and Old World monkeys. J. Hum. Evol. 86, 136–146.
Fernández, P.J., Holowka, N.B., Demes, B., Jungers, W.L., 2016. Form and function of the human and chimpanzee forefoot: implications for early hominin bipedalism. Sci. Rep., 1–10, http://dx.doi.org/10.1038/srep30532.
Franz, T.M., Demes, B., Carlson, K.J., 2005. Gait mechanics of lemurid primates on terrestrial and arboreal substrates. J. Hum. Evol. 48, 199–217.
Gebo, D.L., 1992. Plantigrady and foot adaptation in African apes: implications for hominid origins. Am. J. Phys. Anthropol. 89, 29–58.
Grabowski, M., Hatala, K.G., Jungers, W.L., Richmond, B.G., 2015. Body mass estimates of hominin fossils and the evolution of human body size. J. Hum. Evol. 85, 75–93.
Greiner, T.M., Ball, K.A., 2014. Kinematics of primate midfoot flexibility. Am. J. Phys. Anthropol. 155, 610–620.
Griffin, N.L., Gordon, A.D., Richmond, B.G., Anton, S.C., 2008. Cross-sectional geometric analysis of a foot bone assemblage from Mangaia, Cook Islands. Homo 59, 27–40.
Griffin, N.L., Richmond, B.G., 2005. Cross-sectional geometry of the human forefoot. Bone 37, 253–260.
Haile-Selassie, Y., Saylor, B.Z., Deino, A., Levin, N.E., Alene, M., Latimer, B.M., 2012. A new hominin foot from Ethiopia shows multiple Pliocene bipedal adaptations. Nature 483, 565–569.
Harcourt-Smith, W.E., Throckmorton, Z., Congdon, K.A., Zipfel, B., Deane, A.S., Drapeau, M.S., Churchill, S.E., Berger, L.R., DeSilva, J.M., 2015. The foot of *Homo naledi*. Nat. Commun. 6, 8432, http://dx.doi.org/10.1038/ncomms9432.
Hastie, T., Buja, A., Tibshirani, R., 1995. Penalized discriminant analysis. Ann. Stat. 23, 73–102.
Hatala, K.G., Demes, B., Richmond, B.G., 2016. Laetoli footprints reveal bipedal gait biomechanics different from those of modern humans and chimpanzees. Proc. Roy. Soc. B 283, 1836, http://dx.doi.org/10.1098/rspb.2016.0235.
Hayafune, N., Hayafune, Y., Jacob, H.A.C., 1999. Pressure and force distribution characteristics under the normal foot during the push-off phase in gait. Foot 9, 88–92.
Hicks, J.H., 1954. The mechanics of the foot. II. The plantar aponeurosis and the arch. J. Anat. 88, 25–30.
Jashashvili, T., Dowdeswell, M.R., Lebrun, R., Carlson, K.J., 2015. Cortical structure of hallucal metatarsals and locomotor adaptations in hominoids. PLOS ONE 10, e0117905.
Jones, R.L., 1941. The human foot. An experimental study of its mechanics, and the role of its muscles and ligaments in the support of the arch. Am. J. Anat. 68, 1–39.
Ker, R.F., Bennett, M.B., Bibby, S.R., Kester, R.C., Alexander, R.M., 1987. The spring in the arch of the human foot. Nature 325, 147–149.
Kidd, R.S., 1998. The past is key to the present: thoughts on the origins of human foot structure, function and dysfunction as seen from the fossil record. Foot 8, 75–84.
Kidd, R.S., 1999. Evolution of the rearfoot. A model of adaptation with evidence from the fossil record. J. Am. Podiatr. Med. Assoc. 89, 2–17.
L'Abbe, E.N., Loots, M., Keough, N., 2008. The Matjes River Rockshelter: a description of the skeletal assemblage. South Afr. Archaeol. Bull. 63, 61–68.
Latimer, B., Lovejoy, C.O., 1990. Hallucal tarsometatarsal joint in *Australopithecus afarensis*. Am. J. Phys. Anthropol. 82, 125–133.
Lewis, O.J., 1980a. The joints of the evolving foot. Part II. The intrinsic joints. J. Anat. 130, 833–857.
Lewis, O.J., 1980b. The joints of the evolving foot. Part III. The fossil evidence. J. Anat. 131, 275–298.
Lordkipanidze, D., Jashashvili, T., Vekua, A., Ponce de Leon, M.S., Zollikofer, C.P., Rightmire, G.P., Pontzer, H., Ferring, R., Oms, O., Tappen, M., Bukhsianidze, M., Agusti, J., Kahlke, R., Kiladze, G., Martinez-Navarro, B., Mouskhelishvili, A., Nioradze, M., Rook, L., 2007. Postcranial evidence from early *Homo* from Dmanisi, Georgia. Nature 449, 305–310.
Lovejoy, C.O., Latimer, B., Suwa, G., Asfaw, B., White, T.D., 2009. Combining prehension and propulsion: the foot of *Ardipithecus ramidus*. Science 326, 72e1–72e8, http://dx.doi.org/10.1126/science.1175832.
Marchi, D., 2005. The cross-sectional geometry of the hand and foot bones of the hominoidea and its relationship to locomotor behavior. J. Hum. Evol. 49, 743–761.
Marchi, D., 2010. Articular to diaphyseal proportions of human and great ape metatarsals. Am. J. Phys. Anthropol. 143, 198–207.
Morton, D.J., 1922. Evolution of the human foot. Am. J. Phys. Anthropol. 5, 305–336.
Morton, D.J., 1924. Evolution of the longitudinal arch of the human foot. J. Bone Joint Surg. 6, 56–90.
Morton, D.J., 1935. The Human Foot. Its Evolution, Physiology and Functional Disorders. Columbia University Press, New York.
Nagel, A., Fernholz, F., Kibele, C., Rosenbaum, D., 2008. Long distance running increases plantar pressures beneath the metatarsal heads: a barefoot walking investigation of 200 marathon runners. Gait Posture 27, 152–155.
Nowak, M.G., Carlson, K.J., Patel, B.A., 2010. Apparent density of the primate calcaneo-cuboid joint and its association with locomotor mode, foot posture, and the "midtarsal break". Am. J. Phys. Anthropol. 142, 180–193.
Parr, W.C.H., Chatterjee, H.J., Soligo, C., 2011. Inter- and intra-specific scaling of articular surface areas in the hominoid talus. J. Anat. 218, 386–401.
Pontzer, H., Rolian, C., Rightmire, G.P., Jashashvili, T., Ponce de Leon, M.S., Lordkipanidze, D., Zollikofer, C.P., 2010. Locomotor anatomy and biomechanics of the Dmanisi hominins. J. Hum. Evol. 58, 492–504.
Preuschoft, H., 1969. The mechanical basis of the morphological differences in the skeletons of apes and man. In: Proc 2nd Int. Congr. Primat., Karger, Basel, pp. 160–170.
Proctor, D.J., 2013. Proximal metatarsal articular surface shape and the evolution of a rigid lateral foot in hominins. J. Hum. Evol. 65, 761–769.
Rose, M.D., 1991. The process of bipedalization in hominids. In: Coppens, Y., Senut, B. (Eds.), Origine(s) de la Bipédie chez les Hominidés. CNRS, Paris, pp. 37–48.
Ruff, C.B., 2000. Body size, body shape, and long bone strength in modern humans. J. Hum. Evol. 38, 269–290.
Ruff, C., Holt, B., Trinkaus, E., 2006. Who's afraid of the big bad Wolff?: "Wolff's law" and bone functional adaptation. Am. J. Phys. Anthropol. 129, 484–498.
Ruff, C.B., Trinkaus, E., Walker, A., Larsen, C.S., 1993. Postcranial robusticity in *Homo*. I: Temporal trends and mechanical interpretation. Am. J. Phys. Anthropol. 91, 21–53.
Ryan, T.M., Shaw, C.N., 2015. Gracility of the modern *Homo sapiens* skeleton is the result of decreased biomechanical loading. Proc. Natl. Acad. Sci. U.S.A. 112, 372–377.
Schmitt, D., 2003. Insights into the evolution of human bipedalism from experimental studies of humans and other primates. J. Exp. Biol. 206, 1437–1448.
Schmitt, D., Hanna, J.B., 2004. Substrate alters forelimb to hindlimb peak force ratios in primates. J. Hum. Evol. 46, 237–252.
Schmitt, D., Zeininger, A., Hamrick, E., Snyder, M.L., Kivell, T.L., Wunderlich, R.E., 2016. Gorilla limb kinematics and hominoid locomotor diversity: implications for hominin locomotor evolution. Am. J. Phys. Anthropol. 159 (S 62), 282 (abstract).
Shaw, C.N., Stock, J.T., 2013. Extreme mobility in the Late Pleistocene? Comparing limb biomechanics among fossil *Homo*, varsity athletes and Holocene foragers. J. Hum. Evol. 64, 242–249.
Shaw, C.N., Stock, J.T., Davies, T.G., Ryan, T.M., 2014. Does the distribution and variation in cortical bone along lower limb diaphyses reflect selection for locomotor economy. In: Carlson, K.J., Marchi, D. (Eds.), Reconstructing Mobility – Environmental, Behavioral, and Morphological Determinants. Springer, New York, pp. 49–66.
Smith, R.J., Jungers, W.L., 1997. Body mass in comparative primatology. J. Hum. Evol. 32, 523–559.
Stock, J.T., 2006. Hunter-gatherer postcranial robusticity relative to patterns of mobility, climatic adaptation, and selection for tissue economy. Am. J. Phys. Anthropol. 131, 194–204.
Stokes, I.A., Hutton, W.C., Stott, J.R., 1979. Forces acting on the metatarsals during normal walking. J. Anat. 129, 579–590.
Su, A., Carlson, K.J., 2015. Comparative analysis of trabecular bone structure and orientation in South African hominin tali. Am. J. Phys. Anthropol. 156, 298–299.
Su, A., Wallace, I.J., Nakatsukasa, M., 2013. Trabecular bone anisotropy and orientation in an Early Pleistocene hominin talus from East Turkana, Kenya. J. Hum. Evol. 64, 667–677.
Susman, R.L., 1983. Evolution of the human foot: evidence from Plio-Pleistocene hominids. Foot Ankle 3, 365–376.
Susman, R.L., 1988. New postcranial remains from Swartkrans and their bearing on the functional morphology and behaviour of *Paranthropus robustus*. In: Grine, F.E. (Ed.), Evolutionary History of the "Robust" Australopithecines. Aldine de Gruyter, New York, pp. 149–172.
Susman, R.L., 1989. New hominid fossils from the Swartkrans formation (1979–1986 excavations): postcranial specimens. Am. J. Phys. Anthropol. 79, 451–474.
Susman, R.L., de Ruiter, D., Brain, C.K., 2001. Recently identified postcranial remains of *Paranthropus* and Early *Homo* from Swartkrans Cave, South Africa. J. Hum. Evol. 41, 607–629.

Vereecke, E., D'Aout, K., De Clercq, D., Van Elsacker, L., Aerts, P., 2003. Dynamic plantar pressure distribution during terrestrial locomotion of bonobos (*Pan paniscus*). Am. J. Phys. Anthropol. 120, 373–383.

Voloshina, A.S., Ferris, D.P., 2015. Biomechanics and energetics of running on uneven terrain. J. Exp. Biol. 218, 711–719.

Voloshina, A.S., Kuo, A.D., Daley, M.A., Ferris, D.P., 2013. Biomechanics and energetics of walking on uneven terrain. J. Exp. Biol. 216, 3963–3970.

Ward, C.V., Kimbel, W.H., Johanson, D.C., 2011. Complete fourth metatarsal and arches in the foot of *Australopithecus afarensis*. Science 331, 750–753.

Wearing, S.C., Urry, S.R., Smeathers, J.E., 2001. Ground reaction forces at discrete sites of the foot derived from pressure plate measurements. Foot Ankle Int. 22, 653–661.

Zipfel, B., DeSilva, J.M., Kidd, R.S., 2009. Earliest complete hominin fifth metatarsal. Implications for the evolution of the lateral column of the foot. Am. J. Phys. Anthropol. 140, 532–545.

Zipfel, B., DeSilva, J.M., Kidd, R.S., Carlson, K.J., Churchill, S.E., Berger, L.R., 2011. The foot and ankle of *Australopithecus sediba*. Science 333, 1417–1420.